Changes in Cell Migration and Survival in the Olfactory Bulb of the *pcd/pcd* Mouse

J. Valero, E. Weruaga, A.R. Murias, J.S. Recio, G.G. Curto, C. Gómez, J.R. Alonso

Lab Plasticidad Neuronal y Neurorreparación, Instituto de Neurociencias de Castilla y León, Universidad de Salamanca, E-37007 Salamanca, Spain

Received 28 August 2006; revised 26 September 2006; accepted 11 October 2006

ABSTRACT: **Postnatally, the Purkinje cell degeneration mutant mice lose the main projecting neurons of the main olfactory bulb (OB): mitral cells (MC). In adult animals, progenitor cells from the rostral migratory stream (RMS) differentiate into bulbar interneurons that modulate MC activity. In the present work, we studied changes in proliferation, tangential migration, radial migration patterns, and the survival of these newly generated neurons in this neurodegeneration animal model. The animals were injected with bromodeoxyuridine 2 weeks or 2 months before killing in order to label neuroblast incorporation into the OB and to analyze the survival of these cells after differentiation, respectively. Both the organization and cellular composition of the RMS and the differentiation of the newly generated neurons in the OB were studied using specific markers of glial cells, neuroblasts, and mature neurons. No changes were observed in the cell proliferation rate nor in their tangential migration through the RMS, indicating that migrating neuroblasts are only weakly responsive to the alteration in their target region, the OB. However, the absence of MC does elicit differences in the final destination of the newly generated interneurons. Moreover, the loss of MC also produces changes in the survival of the newly generated interneurons, in accordance with the dramatic decrease in the number of synaptic targets available.** © 2007 Wiley Periodicals, Inc. Develop Neurobiol 67: 839–859, 2007

Keywords: **BrdU; neurogenesis; neuronal degeneration; reelin; rostral migratory stream**

INTRODUCTION

In the adult central nervous system (CNS) of mammals, neuroblasts are mainly generated in two specific regions: the dentate gyrus of the hippocampus and the subventricular zone (SVZ) of the lateral ventricles. In this latter, new cells are directed to the olfactory bulb (OB) (Altman and Das, 1965; Hastings and Gould, 1999). Currently, the implications of this neurogenesis as regards both organization and regeneration capacity in the adult CNS are a hot discussion topic due to the potential application of adult stem cells for neurological repair (Shihabuddin et al., 1999; Peterson, 2002; Lie et al., 2004). Neuronal replacement from endogenous stem cells occurs after neurodegeneration, but it is clearly insufficient (Kay and Blum, 2000; Magavi et al., 2000; Zhang et al., 2001; Arvidsson et al., 2002; Parent et al., 2002). Thus, if possible, strategies must be developed to allow endogenous adult neurogenesis to be functionally relevant in neurodegenerative processes.

Newly generated neuroblasts migrate tangentially from the SVZ to the OB through the rostral migratory stream (RMS). In this tangential migration, astrocytic processes envelop the neuroblasts, to form "glial-tubes", by means of which neuroblasts advance towards the caudal region of the OB (Lois et al., 1996; Peretto et al., 1997). Within the OB, neuro-

Correspondence to: Dr. J.R. Alonso (jralonso@usal.es).

Contract grant sponsor: DGI (Ministerio de Ciencia y Tecnología); contract grant number: BFI 2003-03719.

Contract grant sponsor: Junta de Castilla y León and Fundación FMM.

Published online 21 February 2007 in Wiley InterScience (www.interscience.wiley.com).
DOI 10.1002/dneu.20352

blasts go out of this glial barrier and migrate radially towards both the granule cell layer (GCL) and the glomerular layer (GL), differentiating into interneurons (Altman, 1969; Lois and Álvarez-Buylla, 1994; Carleton et al., 2003). Newly generated neuroblasts mainly give rise to granule cells and periglomerular cells that establish synaptic connections predominantly with mitral cells (MC), the main projection neurons of the OB (Petreanu and Álvarez-Buylla, 2002; Carleton et al., 2003). These OB interneurons play a critical role in the modulation of the olfactory signal by modifying MC activity (Mori et al., 1998, 1999; Carleton et al., 2002; Lledo et al., 2004). Moreover, incorporation of these new neurons into the OB circuitry has been found to be essential for the maintenance of the structure and function of the OB (Gheusi et al., 2000; Rochefort et al., 2002; Zheng et al., 2004).

In this work, the effects of MC loss on the proliferation, tangential migration, radial migration, and differentiation of interneuron precursors and their survival in the adult olfactory system were studied employing the Purkinje cell degeneration (*pcd*) mutant mouse model. *pcd*/*pcd* mice suffer from a selective degeneration of MC with no direct alterations in other neuronal types found in the OB (Greer and Shepherd, 1982), including tufted cells. Neurodegeneration occurs in definite periods, allowing detailed and exact characterization of the degenerative process: selective death of MC begins around postnatal day 60, and at postnatal day 90 most MC have already been lost (Greer and Shepherd, 1982; Valero et al., 2006). Glomerulus activity has been shown to be normal and no effects have been observed in the olfactory nerve axons (Greer and Shepherd, 1982). Furthermore, *pcd*/*pcd* animals are interesting models for neural degeneration, since they are considered to be completely normal at birth, thus avoiding prenatal compensatory mechanisms (Greer and Shepherd, 1982). Accordingly, the *pcd*/*pcd* mouse model allowed us to study how newly generated neuroblasts respond to the lack of their main synaptic target in adults.

METHODS

Animals

C57BL/6J male mice (*Mus musculus,* L. 1758) heterozygous for the pcd^{1J} mutation (*pcd*/+) were obtained from Jackson Laboratories and were mated with DBA/2J females, which did not present the *pcd* alteration. Since *pcd*/*pcd* animals are not useful for breeding, we sorted the littermates according to their genotypes in order to use them as control (+/+) and experimental animals (*pcd*/*pcd*), and to expand the colony (+/*pcd*). The pcd^{1J} allele was associated with the genetic background of the C57BL/6J strain, while the normal allele was associated with the genetic background of the DBA/2J strain. Animal genotyping was performed by PCR amplification of specific microsatellite sequences.

Twelve +/+ mice (eight P104 and four P150) and twelve *pcd*/*pcd* mice (eight P104 and four P150) were used in this study. The animals were kept, handled, and killed in accordance with the Council of the European Communities (directive 86/609/EEC) and current Spanish legislation (RD 1201/2005).

Bromodeoxyuridine Administration

To label proliferating cells, the thymidine analog 5-bromo-2′-deoxyuridine (BrdU; Sigma Chemical Co., St. Louis, MO; 30 μg/g b.w.) was administered intraperitoneally, mixed with the thymidine synthesis inhibitor 5-fluoro-2′-deoxyuridine (Sigma; 3 μg/g b.w.) in 0.1 *M* phosphate buffered-saline, pH 7.3 (PBS). Three consecutive doses of BrdU were injected every 3 h into P90 mice. The animals were injected with BrdU 2 weeks before killing in order to study tangential and radial migration of neuroblasts, or 2 months before killing to analyze survival of newly generated neurons.

Immunohistochemistry

Mice were deeply anesthetized with 1 μL/g b.w. of a mixture of ketamine hydrochloride (3/4; Ketolar, Parke-Davis, Barcelona, Spain) and thiazine hydrochloride (1/4, Rompun, Bayer, Leverkusen, Germany), and then perfused intracardially with 0.9% NaCl, followed by Somogyi's fixative (Somogyi and Takagi, 1982) without glutaraldehyde (5 ml/g b.w.). After perfusion, brains were dissected out, divided into two blocks along a coronal plane using a mouse brain matrix (Electron Microscopy Sciences, PA), and postfixed with the same fixative for 3 h. Brain blocks were then rinsed for 2 h with 0.1 *M* phosphate buffer (PB), pH 7.4, and immersed in 30% (w/v) sucrose in PB until they sank. After cryoprotection, 40 μm-thick coronal sections were obtained with a freezing-sliding microtome (Leica Frigomobil, Jung SM 2000, Nussloch, Germany). The sections were collected in six series in PB and then stored at -20°C in an anti-freezing mixture of 30% glycerol (v/v) and 30% polyethylene glycol (v/v) in PB.

For BrdU immunodetection, sections were rinsed in PBS (3 × 10 min) and then incubated for 1 h at 37°C with 2 *N* HCl to allow DNA denaturation. After HCl incubation, tissues were rinsed in 0.1 *M* borate buffer (pH 8.5, 3 × 10 min) and then in PBS (3 × 10 min). Sections were incubated with a medium made up of 1:5000 rat anti-BrdU (No. MAS250c, Accurate Chemical and Scientific Corporation, NY), 0.2% Triton X-100 (Probus S.A., Barcelona, Spain), and 5% normal goat serum (Vector laboratories, Burlingame, CA) in PBS for 48 h at 4°C. Following this, sections were rinsed in PBS (3 × 10 min) and incubated in 1:1000

biotinylated rat secondary antiserum (Jackson ImmunoResearch Laboratories, West Grove, PA) for 90 min at room temperature. Tissues were rinsed in PBS and incubated in avidin-biotin-peroxidase complex (Kit Elite ABC; 1:200; Vector) for 2 h (room temperature). Finally, sections were rinsed three times in PBS, twice in 0.1 *M* Tris-HCl buffer (pH 7.6), and the reaction product was visualized by incubating the sections in 0.02% 3,3′-diaminobenzidine (w/v) and 0.003% hydrogen peroxide (v/v) in 0.1 *M* Tris-HCl buffer (pH 7.6).

The following primary antibodies were used for single or double immunofluorescence tissue staining with rat anti-BrdU: mouse anti-proliferating cell nuclear antigen (PCNA; 1:3000; No.PC10sc-56, Santa Cruz Biotechnology, Santa Cruz, CA), mouse anti-NeuN (1:5000; No.MAB377, Chemicon International, Temecula, CA), rabbit anti-calretinin (CR; 1:10,000; kindly supplied by Prof. Celio from the University of Fribourg, Switzerland), rabbit anti-neuronal class III β-tubulin (Tuj1; 1:1000; No.PRB-435P, Covance, Berkeley, CA), mouse anti-glial fibrillary acidic protein (GFAP; 1:2000; No.G-3893, Sigma), and mouse anti-reelin (1:1000, No.MAB5366, Chemicon).

For immunofluorescence detection, floating sections were preincubated with 0.13 *M* sodium borohydride for 30 min to remove aldehyde autofluorescence. These sections were then rinsed in PBS (3 × 10 min) and incubated at 4°C for 48 h with a primary antiserum. The incubation medium was made up of 0.2% Triton X-100 (w/v), 5% goat-serum (v/v), and the corresponding antisera diluted in PBS. Finally, the sections were rinsed in PBS (3 × 10 min) and incubated at room temperature in darkness with the corresponding secondary antisera: Cy2-conjugated goat anti-rat IgG, Cy3-conjugated goat anti-mouse IgG, or Cy5-conjugated goat anti-rabbit IgG (all of them at 1:500 from Jackson ImmunoResearch Laboratories). For PCNA staining, floating sections were further fixed at room temperature with Bouin-4%, for 2 h as previously described (Valero et al., 2005). Some sections were incubated for 30 min with 1:2000 propidium iodide (PI; Sigma) diluted in PBS to counterstain all cells. After rising with PBS, sections were mounted with an antifading medium (Valero et al., 2005).

Terminal Deoxynucleotidyl Transferase-Mediated Biotin-dUTP Nick End Labeling

To detect apoptotic bodies, tissue sections were postfixed with 4% paraformaldehyde in PB for 20 min. After the sections had been rinsed (PBS 3 × 10 min), they were treated with ethanol/acetic acid (2:1) at −20°C for 5 min. Then, tissues were rinsed in PBS (3 × 10 min) and permeated at room temperature for 15 min with 0.2% Triton X-100 diluted in 0.1% sodium citrate (w/v). After permeation, the TUNEL technique was carried out as previously described (Gascon et al., 2005). Briefly, tissues were rinsed in PBS (2 × 5 min) and immersed for 30 min in dUTP Nick End Labeling (TUNEL) buffer made up of 30 m*M* Tris-HCl buffer (pH 7.2), 140 m*M* sodium cacodylate, 1 m*M* cobalt chloride, and 0.3% Triton X-100. Tissues were then incubated at 37°C with the TUNEL reaction mixture containing 800 U/ml of terminal transferase (Roche Diagnostics, Mannheim, Germany) and 1 μM biotin-16-2′-deoxy-uridine-5′-triphosphate (Roche) for 2 h, both diluted in TUNEL buffer. Finally, sections were rinsed in PBS (3 × 10 min), incubated at room temperature in darkness with Cy2-conjugated streptavidin (1:500; Jackson ImmunoResearch Laboratories), and counterstained with 1:2000 PI. After three rinses with PBS, the sections were mounted with antifading medium and coverslipped.

Quantitative Analysis

The percentage of PCNA-positive cells was studied at three different levels. Equivalent serial sections from each brain were chosen considering anatomical landmarks and their relative positions to Bregma (Hof et al., 2000). These zones correspond to SVZ [Bregma 0.20 mm; Fig. 1(A,B)], RMS [Bregma 1.50 mm; Fig. 1(A,C)], and RMS-OB [Bregma 3.80 mm; Fig. 1(A,D)]. The percentage of PCNA-positive cells was estimated by counting the total number of cells (stained with PI) and the number of PCNA-positive cells present on a single plane image obtained with a confocal microscope at 40× (Leica TCS SP spectral confocal microscope; Leica, Mannheim, Germany).

Quantification of BrdU-positive (BrdU+) cells in the OB and estimations of layer areas were performed using Neurolucida software (MicroBrightField, Williston, VT). The areas of the different OB layers were measured in 40 μm-thick serial sections at 240 μm rostrocaudal intervals. The volumes of the layers were calculated using TableCurve 2D v5.01 (AISN Software, Mapleton, OR). The density of BrdU+ cells in the OB was estimated by obtaining the mean density from two representative levels, selected as reported previously (Weruaga et al., 1999). The OB was divided into five rostrocaudal levels and the third and fourth levels were selected for the analysis, since they were the levels containing the largest surface for all layers analyzed. The total number of BrdU+ cells in each layer was corrected using an Abercrombie-based method, as previously reported (Petreanu and Álvarez-Buylla, 2002).

Equivalent OB sections were chosen from control and mutant animals to determine the percentage of BrdU+ cells expressing different neuronal markers. The analysis was performed using plane images from dorsal, lateral, ventral, and medial OB quadrants obtained with confocal microscopy. Confocal images were analyzed using the Leica confocal software (v2.61) and imageJ 1.37i (Rosband, W. S., National Institutes of Health, Bethesda, MA). The number of CR+ cells and MC was estimated using this procedure and the Abercrombie-based method.

Epifluorescence microscopy was employed to count TUNEL+ bodies. Quantification of these TUNEL+ bodies in the OB was performed using the Abercrombie-based method. Since the number of TUNEL+ bodies per 40 μm-thick slice was very low, their density in the OB was estimated obtaining the mean density of all OB sections in a one-in-six series (see the immunohistochemistry procedures).

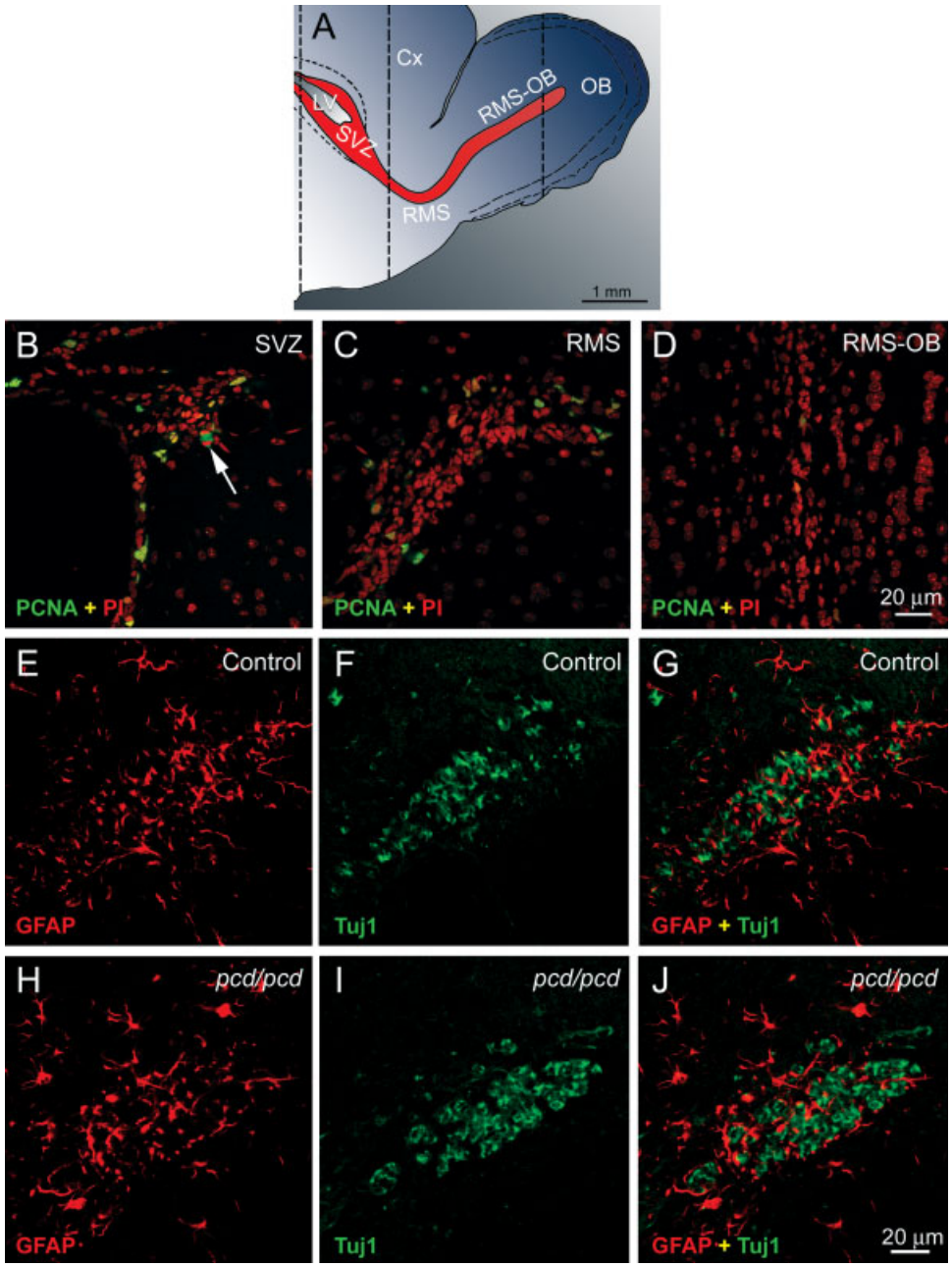

Figure 1 MC loss does not affect cellular proliferation or cellular organization in the RMS. (A) Schematic sagittal view of the rostral region of the adult mouse brain. The RMS pathway is represented in red. Shaded lines show the rostrocaudal levels chosen to study proliferation. (B–D) Confocal microscopy images of the three rostrocaudal levels indicated in (A), and stained for PCNA (green and yellowish tones for colocalization with PI) and counterstained with PI (red) from a P104 control mouse. The arrow in (B) points to a mitotic cell in the SVZ stained with PCNA. No differences in the percentage of PCNA+ cells were observed between control and *pcd*/*pcd* mice (Table 1). Scale bar in (D) also applies to (B,C). (E–J) Confocal microscopy images of coronal sections of the RMS from a P104 control mouse (E–G) and a *pcd*/*pcd* mouse (H–J) stained for GFAP (red) and Tuj1 (green). GFAP staining demonstrates the astrocytic component of the RMS and was similar in control [(E), red in (G)] and *pcd*/*pcd* mice [(H), red in (J)]. Tuj1 labeling stained neuroblasts of the RMS and was similar in control [(F), green in (G)] and *pcd*/*pcd* mice [(I), green in (J)]. No abnormalities were observed in the RMS structure of *pcd*/*pcd* mice [compare (G) and (J)]. Scale bar in (J) applies to (E–I). Cx, cortex; GFAP, glial fibrillary acidic protein; LV, lateral ventricle; OB, olfactory bulb; PCNA, proliferating cell nuclear antigen; PI, propidium iodide; RMS, rostral migratory stream; RMS-OB, terminal region of the RMS in the caudal OB; SVZ, subventricular zone. [Color figure can be viewed in the online issue, which is available at www.interscience.wiley.com.]

Statistical Analyses

Statistical differences were assessed by *t* test or the one-way ANOVA and Student-Newman-Keuls *post hoc* analysis when comparing more than two groups. The level of significance was set at $p < 0.05$. When the statistical groups included both males and females (P104 animals, $n = 4$ for males and $n = 4$ for females), possible differences between them were tested and were found to be not significant. Accordingly, male and female data were grouped for the final statistical analysis in these groups.

RESULTS

Cell Proliferation

The loss of MC could affect both the organization and proliferation of neuronal precursors into the RMS. In light of this, the percentages of proliferating cells in three regions of the adult CNS were quantified and compared between the mutant and control animals [(Fig. 1(A–D)]: namely, the dorsal horn of the SVZ, the RMS, and the end region of the RMS within the OB (RMS-OB). PCNA immunofluorescence was employed to detect proliferating cells, combined with PI counterstaining [Fig. 1(B–D)]. PCNA immunodetection stains only the proliferating cells in the regions studied (Valero et al., 2005). The percentage of PCNA-positive cells in these three regions was not significantly different between the control and *pcd*/*pcd* mice (Table 1). These results indicate that MC loss does not affect cell generation in the regions studied.

Tangential Migration

Since no changes in cell proliferation in the *pcd*/*pcd* RMS were detected, it may be inferred that the same number of neuroblasts must have reached the control or *pcd*/*pcd* OBs. However, alterations of the RMS structure could affect the tangential migration of cells through this pathway, hindering the arrival of new neuroblasts to the *pcd*/*pcd* OB. The possible structural abnormalities in the RMS of *pcd*/*pcd* mice were analyzed by immunodetection of GFAP and β-III-tubulin (detected with Tuj1 antibody). GFAP is present in the astrocytes forming the glial tubes of the SVZ and RMS, while in Tuj1 stains migrating neuroblasts (Doetsch et al., 1997). The SVZ, RMS, and RMS-OB of the *pcd*/*pcd* mice did not exhibit significant structural abnormalities as seen with either GFAP or Tuj1 immunolabeling [Fig. 1(E–J)]. Newly generated cells in the SVZ of adult mice populate the OB 12 days after their birth (Lois and Álvarez-Buylla, 1994; Petreanu and Álvarez-Buylla, 2002). To determine the number of precursors that reached the OB, BrdU was injected into mice at P90, and to ensure that most of these migrating cells had indeed reached the OB, the animals were killed 14 days after BrdU administration and the number of BrdU+ cells was estimated in the OB. This approach allowed us to discriminate possible changes in tangential migration caused by the loss of MC. No significant differences in the total number of BrdU+ cells in the OB of control and mutant mice were observed (control: 33,194 ± 3892 BrdU+ cells, $n = 8$; *pcd*/*pcd*: 29,948 ± 3426 BrdU+ cells, $n = 7$; mean ± SDM), indicating that the tangential migration of neuronal precursors through the RMS is not affected by MC loss.

Table 1 ***pcd*/*pcd* Mice Show Normal Cell Proliferation**

Region	Control ($n = 8$)	*pcd*/*pcd* ($n = 8$)
SVZ	28.0 ± 8.2	29.6 ± 5.8
RMS	27.9 ± 4.5	27.1 ± 5.5
RMS-OB	3.7 ± 3.0	5.0 ± 3.6

Percentage of PCNA+ referred to the total number of cells in each region. Data represent the mean ± SDM.

Radial Migration in Control and *pcd*/*pcd* Mice

To study radial migration through the OB, we analyzed the distribution of BrdU+ cells 14 days after BrdU administration in three areas (Fig. 2): the inframitral layers (IML), the external plexiform layer (EPL), and the GL. The IML include the MC layer (MCL), the inner plexiform layer, the GCL, and the RMS-OB. These layers were grouped, because their limits are sometimes diffuse in the *pcd* mutants and because of the disappearance of MC. To compare the radial spread across the OB between the control and mutant animals, the percentage of total BrdU+ cells in each area was determined. The distribution of BrdU+ cells was significantly different between the control and *pcd*/*pcd* mice. Most BrdU+ cells in the control and mutant mice were located in the IML (Table 2; Fig. 2). However, the percentage of BrdU+ cells, referred to the total number of BrdU+ cells throughout the OB, was lower in the IML of the *pcd*/*pcd* mice while it was higher in the GL [Table 2; Fig. 2(E)]. Since the control and *pcd*/*pcd* mice showed the same total number of cells in the OB, these changes in the distribution of BrdU+ cells may be attributed to differences in the radial migration of cells. The data obtained reveal that the loss of MC in *pcd*/*pcd* mutant mice leads to a change in the radial migration of neuro-

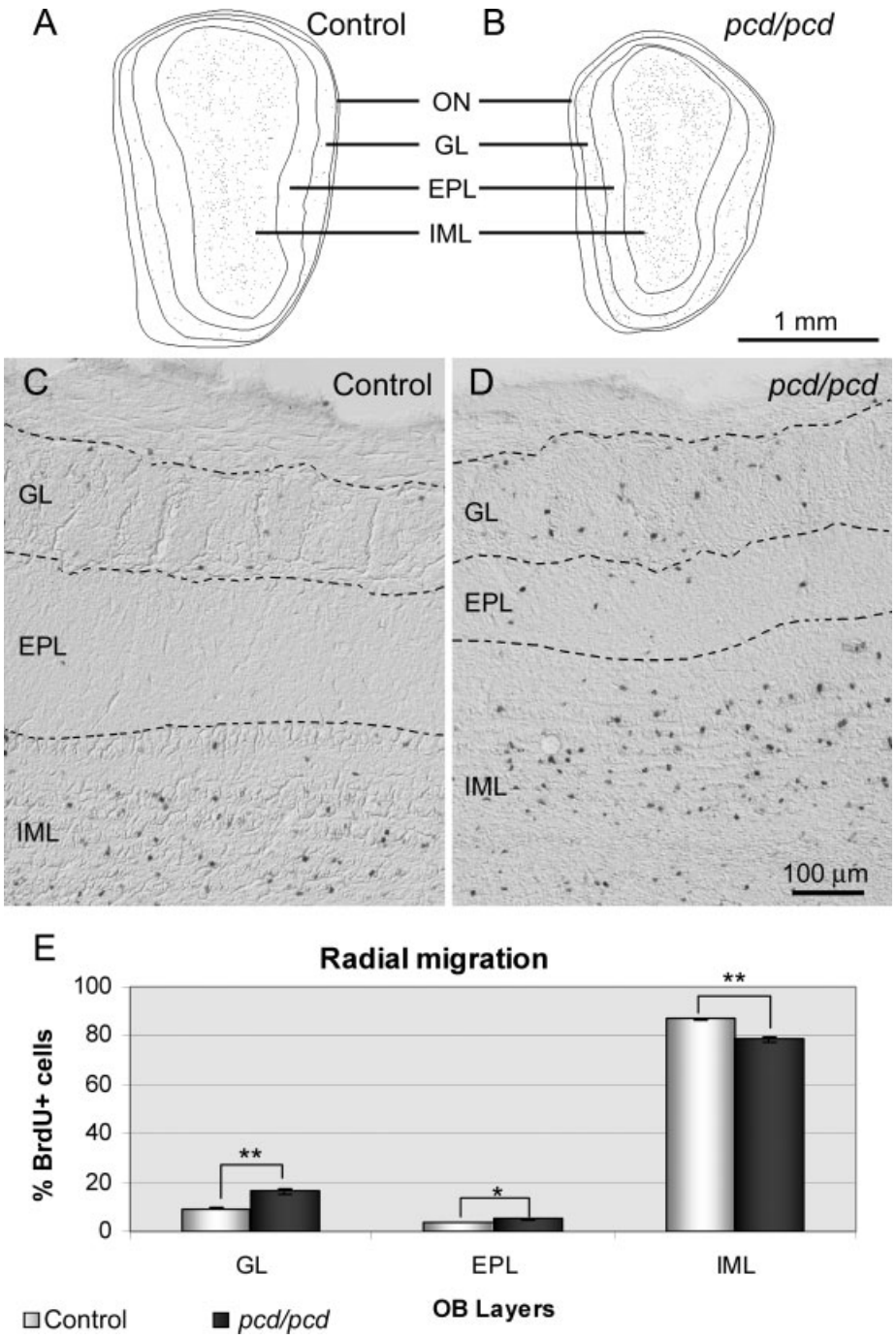

Figure 2 MC loss alters radial migration. (A–B) Drawings of coronal sections from the OB of a control (A) and a *pcd*/*pcd* (B) mouse. Dots represent BrdU+ cells and lines delimit the different regions analyzed. Scale bar in (B) applies to (A). (C–D) BrdU immunostaining of coronal sections from a control (C) and a *pcd*/*pcd* (D) mouse injected with BrdU 14 days before sacrifice. Shaded lines delimit the different regions analyzed. Note the higher number of BrdU+ cells (dark dots) in the GL of the *pcd*/*pcd* mouse and the clear reduction in its EPL width. Scale bar in (D) applies to (C). (E) Quantitative analysis of the distribution of BrdU+ cells in the OB. Percentage of BrdU+ cells in each layer is referred to the total number of BrdU+ cells throughout the OB. A lower percentage of BrdU+ cells was encountered in the IML of the *pcd*/*pcd* mice, whereas a higher percentage of BrdU+ cells was obtained in their EPL and GL. Considering that the total number of BrdU+ cells in the OB was similar in the control and *pcd*/*pcd* mice 14 after BrdU administration (Table 2), these data indicate that more cells have migrated radially from the inner to the outer layers in the *pcd*/*pcd* OB. $n = 8$ for control and $n = 7$ for *pcd*/*pcd* mice. *$p < 0.05$, **$p < 0.01$. EPL, external plexiform layer; GL, glomerular layer; IML, inframitral layers; OB, olfactory bulb.

Table 2 *pcd/pcd* Mice Exhibit Changes in Radial Migration

Layer	Control ($n = 8$)	*pcd/pcd* ($n = 7$)
GL	9.3 ± 1.2	16.4 ± 2.2**
EPL	3.8 ± 0.9	5.2 ± 0.9*
IML	86.9 ± 1.5	78.4 ± 2.6**

Percentage of BrdU+ cells in each OB layer 14 days after BrdU administration. Data represent the mean ± SDM.

* $p < 0.05$ and ** $p < 0.01$ versus control data.

nal precursors, increasing the numbers of those that continue to migrate and reach the GL.

Distribution of BrdU+ Cells Along the Inframitral Layers 14 Days After BrdU Administration

The IML were delimited by dividing it into five concentric sectors (I to V) in order to analyze the distribution of BrdU+ cells along the IML (Table 3; Fig. 3). The areas of these sectors (from sector I to sector V) comprised 36, 28, 20, 12, and 4% of the whole IML area. Although the area of sector I was larger than that of sector II, our results revealed a higher accumulation of BrdU+ cells in sector II of both the control and *pcd/pcd* mice than in sector I [Table 3; Fig. 3(B)]. This result must be related to the presence of the inner plexiform layer in sector I, which is not the final destination for interneuron precursors. The percentage of BrdU+ cells was significantly different between similar sectors of the control and *pcd/pcd* mice [Table 3, Fig. 3(B)]. A higher percentage of labeled cells was detected in the upper sector (I) of the *pcd/pcd* mice and a lower percentage in the deeper sectors (IV and V), while the percentages in sectors II and III were not significantly different [Table 3; Fig. 3(B)]. These data confirm that a higher number of neuroblasts migrate to superficial sectors in *pcd/pcd* mice as compared with control animals, i.e., the newly generated cells continue their radial migration further, and reach more superficial destinations than do the same cells in controls. Our results suggest that MC play a key role in neuroblast radial migration through the IML in adult mice.

Expression of Reelin in the OB of *pcd/pcd* Mice

Reelin is an extracellular matrix glycoprotein mainly expressed by MC in the OB (D'Arcangelo et al., 1995; Hack et al., 2002; Pappas et al., 2003). It is essential for both ordered neuronal migration and normal layering (D'Arcangelo et al., 1995; Ogawa et al., 1995). Reelin expression has been observed in the GL, EPL, MCL, and GCL (Hack et al., 2002; Pappas et al., 2003). Moreover, a decreasing reelin gradient from the MCL to the RMS-OB has been reported (Hack et al., 2002). All these data strongly suggest that reelin would be involved in the radial migration of neuroblasts that reach the OB through the RMS. In light of this, we analyzed reelin expression in the OB of *pcd/pcd* mice. In control mice, reelin protein was detected in periglomerular cells of the GL, tufted cells of the EPL, MC (Fig. 4), and granule cells (not shown); in contrast, no expression was found in RMS-OB cells. In the *pcd/pcd* mice, the expression pattern of reelin coincided with that observed in the control animals, except for the lack of MC, an important population of reelin-expressing neurons [Fig. 4(B)]. However, reelin expression in *pcd/pcd* OB slices seemed to be higher in the GL and EPL (Fig. 4) in view of the increase in cell density, due to the reduction in the volume of the *pcd/pcd* OB (see volumetric analyses). These data suggest the existence of altered gradients of reelin, including a stronger periglomerular signal and an

Table 3 *pcd/pcd* Mice Exhibit Changes in the Distribution of BrdU+ Cells Along the IML

IML Sector	Time After BrdU Administration			
	14 Days		60 Days	
	Control ($n = 8$)	*pcd/pcd* ($n = 7$)	Control ($n = 4$)	*pcd/pcd* ($n = 4$)
I	22.6 ± 2.6	26.0 ± 1.3*	22.1 ± 2.0	28.8 ± 3.5**
II	30.2 ± 1.3	32.6 ± 1.6	32.7 ± 2.5	36.7 ± 1.8**
III	24.1 ± 1.0	22.6 ± 1.2	23.5 ± 2.0	22.3 ± 1.7
IV	16.8 ± 1.4	14.4 ± 1.2**	17.0 ± 1.2	9.4 ± 0.9**
V	6.3 ± 1.2	4.5 ± 1.3*	4.7 ± 0.8	2.7 ± 0.6**

Percentage of BrdU+ cells in each IML sector referred to the total number of BrdU+ cells throughout the IML. Data represent the mean ± SDM.

* $p < 0.05$ and ** $p < 0.01$ versus control data at the same time after BrdU administration.

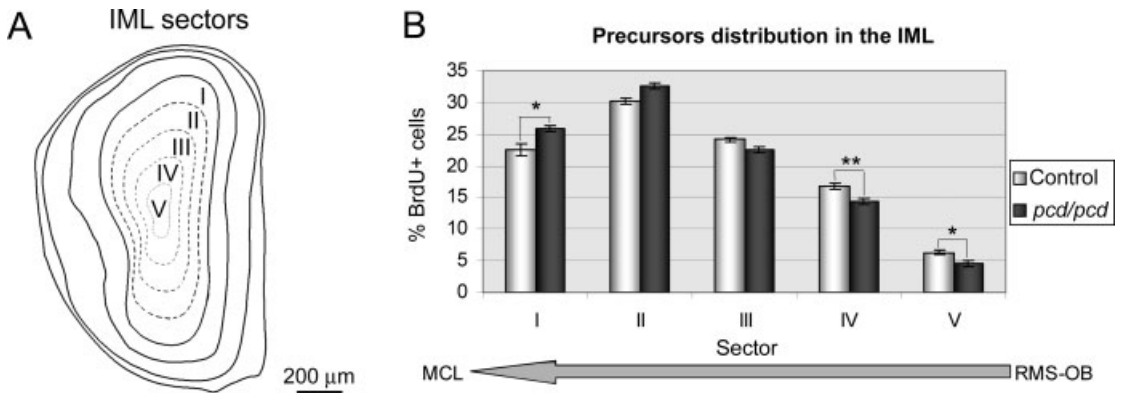

Figure 3 MC loss changes the distribution of newly generated cells in inframitral layers. (A) Drawing of a section from a control mouse showing the different sectors established (I to V) to analyze the distribution of BrdU+ cells in the IML. Shaded lines delimit different sectors. (B) Quantitative analysis of the distribution of BrdU+ cells in the IML 14 days after BrdU administration. Percentage of BrdU+ cells in each sector is referred to the total number of BrdU+ cells in the IML. Sector I of *pcd*/*pcd* mice showed a higher percentage of BrdU+ cells, whereas sectors IV and V showed a lower percentage. This indicates that in *pcd*/*pcd* mice a higher proportion of cells migrate from the inner to the outer regions of the IML. $n = 8$ for control and $n = 7$ for *pcd*/*pcd* mice. *$p < 0.05$, **$p < 0.01$. IML, inframitral layers; MCL, mitral cell layer; RMS-OB, terminal region of the RMS in the caudal OB.

almost complete loss of reelin in the MCL in the OB of the *pcd*/*pcd* mice.

Early Neuronal Differentiation of Newly Generated Cells

The characterization of the early differentiation of BrdU+ cells was carried out by double or triple immunofluorescent staining with glial and neuronal markers. To analyze possible gliogenesis within the OB, we tested the colocalization of BrdU with GFAP, a marker of astrocytes (Bignami and Dahl, 1974). We found that only a few BrdU+ cells were GFAP+ in the OB of either control or mutant mice. Thus, the new generation of astrocytes was equally low in the OB of both the control and *pcd*/*pcd* mice, ruling out possible gliosis reactions caused by MC degeneration. NeuN was employed as a general neuronal marker (Mullen et al., 1992) and its colocalization with BrdU was analyzed to identify newly generated neurons. The percentages of BrdU+ cells colocalizing with NeuN in the GL and IML were similar in both the control and *pcd*/*pcd* mice (Table 4). Also, CR was employed as a specific neuronal marker, since it is expressed by particular sets of neurons located in the GCL and the GL (Resibois and Rogers, 1992; Qin et al., 2005). CR was expressed by some BrdU+ cells and, also, no significant differences were observed between the colocalization percentages in the IML or in the GL of the control and mutant mice (Table 4). A triple immunofluorescence technique for the detection of BrdU, NeuN, and CR was used to determine how many BrdU+ cells had a differentiated neuronal phenotype. The percentage of BrdU+ cells that expressed, at least, one of both neuronal markers in the two regions analyzed—the IML and GL of control and *pcd*/*pcd* mice (Table 4)—was similar. These data demonstrate that MC loss did not affect neuronal differentiation of new cells being incorporated into the OB.

Survival of Newly Generated Cells Incorporated into the OB

The number of BrdU+ cells present in the OB was quantified 60 days after BrdU administration with a viewing to study the extent of the death of these cells. The number of surviving BrdU+ cells throughout the OB was significantly lower in the *pcd*/*pcd* mice as compared with controls [control, 26,706 ± 1749 BrdU+ cells; *pcd*/*pcd*, 13,431 ± 689 BrdU+ cells; $n = 4$; $p < 0.01$; Fig. 5(A–C)]. This decrease in the number of BrdU+ cells was mainly due to a significant reduction in the number of BrdU+ cells in the IML of the *pcd*/*pcd* mice [Table 5; Fig. 5(C)]. However, no significant differences were observed between the number of BrdU+ cells around the glomeruli of *pcd*/*pcd* and control mice. The final number of newly generated neurons incorporated into the OB depends on two main factors: first, the incorporation of cells into a particular OB layer, and second, their

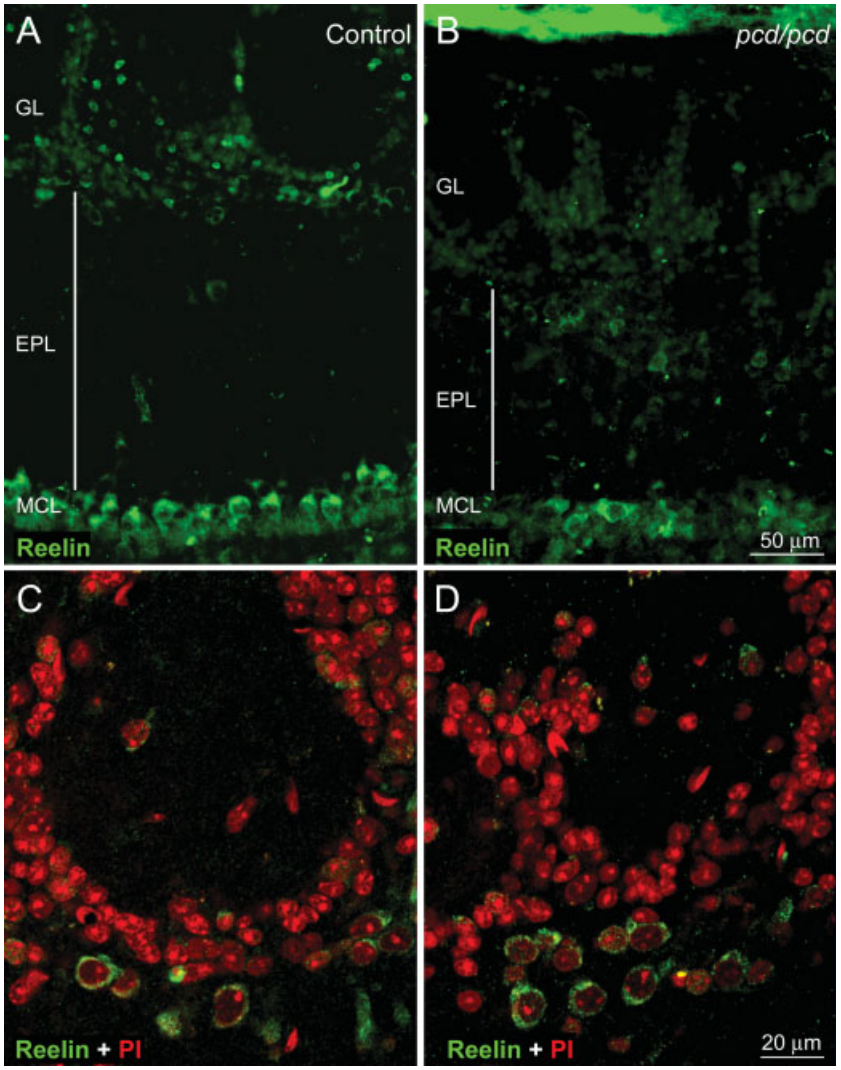

Figure 4 Reelin expression in the *pcd*/*pcd* mouse OB. (A,B) Epifluorescence microscopy images from coronal sections of the OB of a P104 control (A) and a P104 *pcd*/*pcd* mouse (B) stained for reelin. Reelin is expressed by juxtaglomerular, tufted, mitral, and granule cells (A). Note the reduction in the number of MC in the *pcd*/*pcd* OB, the reduction in its EPL width, and the increase in the density of reelin positive elements close to its GL (B). Scale bar in (B) applies to (A). (C,D) Confocal microscopy images from the GL of a control (C) and a *pcd*/*pcd* mouse (D) stained for reelin (green) and counterstained with PI (red). Note the higher proportion of reelin-positive cells (green) in the GL of the *pcd*/*pcd* mouse (D) in comparison with the GL of the control animal (C). Scale bar in (D) applies to (C). EPL, external plexiform layer; GL, glomerular layer; MCL, mitral cell layer; PI, propidium iodide. [Color figure can be viewed in the online issue, which is available at www.interscience.wiley.com.]

survival rate. Thus, the percentage of BrdU+ cells after 60 days ($BrdU_{60}$) with respect to those stained only 14 days after injection ($BrdU_{14}$) was calculated to estimate the survival of newly generated cells incorporated into the OB (% of survivor cells = $BrdU_{60} \times 100/BrdU_{14}$). This rate was significantly higher in the control mice as compared with the *pcd*/*pcd* animals [control, 80.4 ± 5.3%; *pcd*/*pcd*, 44.8 ± 2.3%, $p < 0.01$; $n = 4$; Fig. 5(D)]. The survival of newly generated cells was different within the different areas (GL, EPL, and IML) when analyzed separately in the *pcd*/*pcd* mouse OB (GL, 46.91 ± 3.37%; EPL, 27.31 ± 7.18%; IML, 50.73 ± 5.44%; $n = 4$) and in comparison with the control animals [GL, 74.93 ± 8.15%; EPL, 89.61 ± 21.08%; IML, 82.64 ± 8.23%; $n = 4$; Fig. 5(D)].

Table 4 *pcd/pcd* Mice do not Exhibit Changes in Neuronal Differentiation 14 Days After BrdU Administration

	Layer			
	GL		IML	
Markers	Control	*pcd/pcd*	Control	*pcd/pcd*
BrdU/NeuN	29.8 ± 5.8	34.6 ± 6.0	82.5 ± 5.5	79.3 ± 5.7
BrdU/CR	38.3 ± 5.9	29.1 ± 10.8	31.0 ± 2.5	26.8 ± 6.6
BrdU/NeuN or CR	58.7 ± 8.5	54.2 ± 10.3	87.7 ± 4.0	85.6 ± 3.6

Percentage of cells colocalizing BrdU with neuronal markers referred to the total number of BrdU+ cells in each layer. Data represent the mean ± SDM. $n = 4$ in all groups.

The selection process of newly generated cells in the OB is related to apoptotic mechanisms (Yamaguchi and Mori, 2005). To corroborate the above results concerning cell survival, we stained apoptotic bodies using the TUNEL technique. We analyzed the number of TUNEL+ bodies in the GL and IML of the control and *pcd/pcd* mice. The number of TUNEL+ bodies in the EPL was not analyzed owing to the extremely low frequency of apoptotic bodies detected in this layer. Significant differences ($p < 0.01$) in the number of TUNEL+ bodies in the GL were found between the control and *pcd/pcd* mice (control, 48.8 ± 31.4; *pcd/pcd*, 116.98 ± 16.21, $n = 4$; Fig. 6). Significant differences ($p < 0.01$) were also observed in the IML between the control and *pcd/pcd* mice (control, 432.0 ± 94.9; *pcd/pcd*, 786.1 ± 140.4; $n = 4$; Fig. 6). These data show that a loss of MC reduces the survival of newly generated cells in all OB layers, thus increasing apoptotic events. Furthermore, our results indicate that the loss of MC affects the final destination of newly generated cells in the OB. Interestingly, the degeneration of MC did not elicit changes in the final number of surviving cells in the GL, where these cells may be contacted by olfactory axons, although it decreased to a considerable extent the number of newly incorporated cells into the IML, where their main synaptic target are MC [Table 5; Fig. 5(C)].

Survival of Newly Generated Cells in Different Zones of IML

The distribution of BrdU+ cells across the IML was analyzed as described earlier, dividing the IML into five sectors [Fig. 3(A)]. The percentage of BrdU+ cells was significantly different between the sectors of the control and *pcd/pcd* mice [Table 3, Fig. 7(A)]. A higher percentage of cells was found in the external-most sectors (I and II) of the *pcd/pcd* mice and a lower percentage in deeper ones (IV and V), while there were no significant differences in sector III [Table 3, Fig. 7(A)]. These data confirm the preference of newly generated cells for final incorporation into the superficial sectors of the IML. The final incorporation of newly generated cells into a given layer (sector) depends on their ability to migrate and survive. In light of this, we studied the existence of survival rate differences among sectors (I to V) in the control group. In the control animals, only sector V showed a significantly ($p < 0.05$) lower survival of new cells in comparison with the other sectors [sector I, 80.7% ± 10.2%; sector II, 89.3% ± 9.3%; sector III, 81.2% ± 11.4%; sector IV, 84.2% ± 10.5%; and sector V, 62.3% ± 14.3%; the data indicate the means of the % of cells that survived in each sector ± SDM, $n = 4$; Fig. 7(B)]. However, in the IML of the *pcd/pcd* mice two sectors (IV and V) showed a significantly ($p < 0.01$) lower survival rate of new cells in comparison with the other IML sectors [sector I, 56.0% ± 3.3%; sector II, 57.4% ± 8.2%; sector III, 50.4% ± 8.3%; sector IV, 33.4% ± 6.5%; sector V, 29.7% ± 6.8%; the data indicate the means of the % of cells that survived in each sector ± SDM; $n = 4$; Fig. 7(B)]. The significant reduction in cell survival in the *pcd/pcd* IML in comparison with the controls has been described earlier [Fig. 5(D)]. The relative survival in each IML sector was calculated in order to study whether the loss of MC exerted a stronger effect in any given sector of the IML. The relative survival in each IML sector was obtained as the rate between the survival in the sector and general survival throughout the IML (relative survival = sector survival/whole IML survival). The only sector that exhibited a significant difference between the control and *pcd/pcd* mice was sector IV [Fig. 7(C)], which showed a higher reduction in relative survival in the *pcd/pcd* mice (1.0 ± 0.1 in control mice vs. 0.7 ± 0.1 in *pcd/pcd* mice, mean ± SDM, $n = 4$). The relative survival of cells in sector V of the *pcd/pcd* mice was similar to that obtained in the controls [Fig. 7(C)]. This shows that the survival of cells in sector V of the *pcd/pcd* mice and most other sectors (except for sector IV) was equally reduced by the loss of MC. The

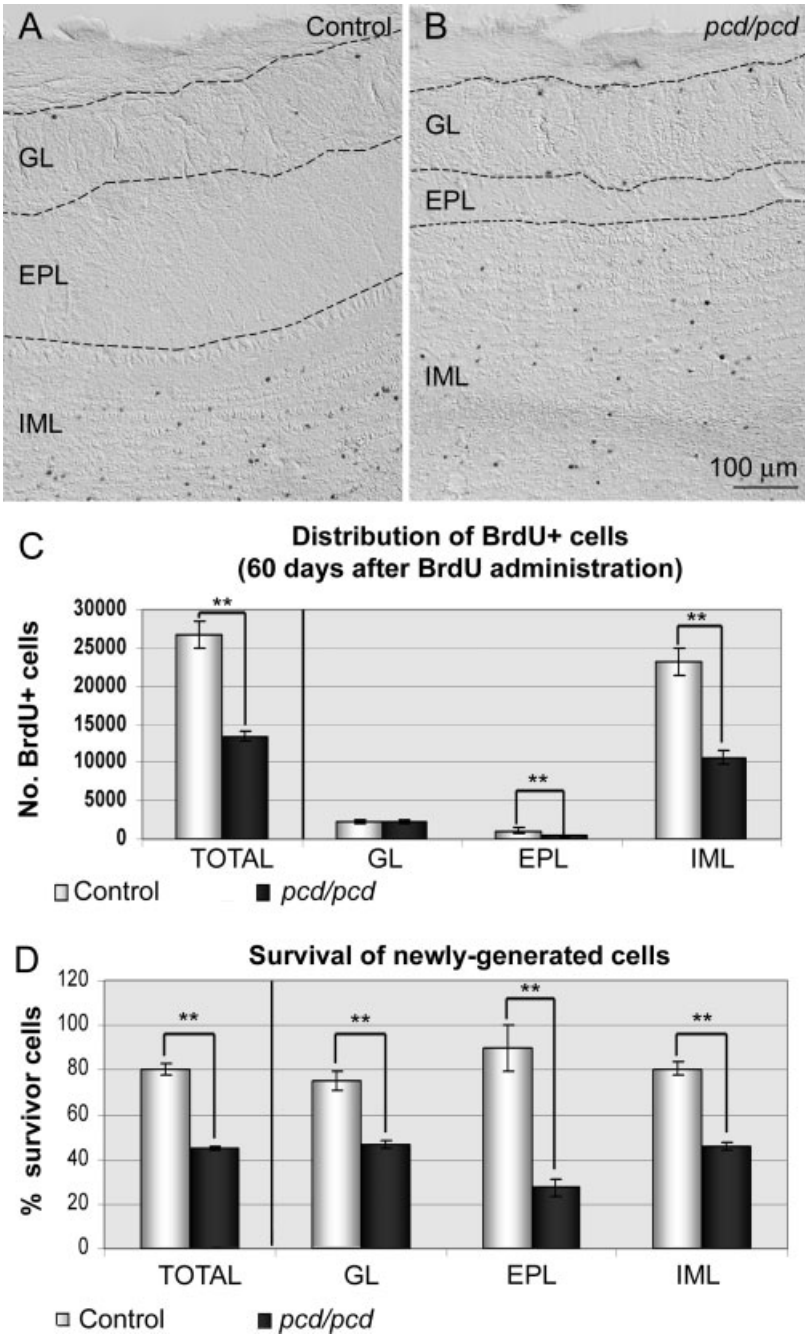

Figure 5 MC loss decreases the survival of newly-generated cells. BrdU immunostaining of coronal sections from a control (A) and a *pcd*/*pcd* (B) mouse injected with BrdU 60 days before they were killed. Shaded lines delimit the different regions analyzed. Note the lower number of BrdU+ cells (dark dots) in the IML of the *pcd*/*pcd* mouse (B). Scale bar in (B) applies to (A). (C) Quantitative analysis of BrdU+ cells distribution in the OB of the control and *pcd*/*pcd* mice. A lower number of BrdU+ cells was obtained throughout the OB of the *pcd*/*pcd* mice as compared with control animals, mainly due to the reduction in BrdU+ elements in the IML. Note that the number of BrdU+ cells in the GL of control and *pcd*/*pcd* mice was similar. (D) Quantitative analysis of the percentage of surviving cells in the OB of control and *pcd*/*pcd* mice. All layers present a reduced percentage of surviving cells in the *pcd*/*pcd* OB. $^{**}p < 0.01$. EPL, external plexiform layer; GL, glomerular layer; IML, inframitral layer.

Table 5 *pcd/pcd* Mice Exhibit Changes in the Final Number of BrdU+ Cells

Layer	Control ($n = 4$)	*pcd/pcd* ($n = 4$)
GL	2,308 ± 251	2,296 ± 165
EPL	1,126 ± 265	429 ± 113**
IML	23,272 ± 1,774	10,706 ± 810**

Number of $BrdU^+$ cells 60 days after BrdU administration. Data represent the mean ± SDM.

** $p < 0.01$ versus control data.

data obtained indicate that the loss of MC causes a massive loss of many newly generated cells in the IML and that most remaining cells are located more superficially.

Neuronal Fate of Surviving Newly Generated Cells

As reported earlier, most BrdU+ cells expressed one or both neuronal markers: NeuN or CR, indicating that they are "mature" neurons. To check the neuronal phenotype of survivor BrdU+ cells, a triple immunofluorescence technique aimed at detecting BrdU, NeuN, and CR was carried out 60 days after BrdU administration. Most BrdU+ cells in the IML were stained with either of both markers (NeuN or CR) or colocalized both. No significant differences between the control and mutant mice were found in the IML (Table 6). However, the percentage of BrdU+ cells showing NeuN immunostaining was significantly higher in the GL of the *pcd/pcd* mice, whereas the percentage of BrdU+ cells expressing CR was equal in this layer (Table 6). The increase in the number of cells double-labeled for BrdU and NeuN in the GL of the *pcd/pcd* mice cannot be clearly attributed to changes in the differentiation or functionality of these cells owing to the lack of studies addressing the functional implications of NeuN expression in neurons. These results clearly indicate that 60 days after BrdU administration most BrdU+ cells differentiate into neurons. It may also be concluded that the loss of MC reduces the number of newly generated cells expressing CR in the IML but does not produce either a positive or negative specific selection of this cell population.

CR is expressed by MC and interneurons located in the GCL and the GL of the OB (Resibois and Rogers, 1992; Qin et al., 2005). According to the aforementioned data concerning the expression of CR by newly generated cells in the OB and the differences in the survival of cells observed in this work, a possible effect in the whole population of CR+ interneurons in the OB can be postulated. To tackle this issue, the number of CR+ cells was analyzed in both the GL and IML of control and *pcd/pcd* mice. The number of CR+ cells in the *pcd/pcd* GL was similar to that of the control mice, while the number of CR+ cells in the IML was significantly lower in the *pcd/pcd* mice (control GL, 711,402 ± 60,218 CR+ cells; *pcd/pcd* GL, 649,497 ± 86,047 CR+ cells; control IML, 714,315 ± 107,375 CR+ cells; *pcd/pcd* IML, 258,845 ± 52,235; $p < 0.01$; mean ± SDM, $n = 4$, Fig. 8). These data are consistent with the findings obtained in this work as regards newly generated cells, indicating that the population of CR+ cells in the GL is not affected by the loss of MC, while the IML population is highly dependent on the existence of MC.

Volume Changes in the OB of *pcd/pcd* Mice

Our analysis indicates that 29.25% ± 3.09% of the MC survive in the OB of the *pcd/pcd* mice, with no differences between animals from either age studied (P104 and P150). Since MC loss has been reported to induce volumetric changes in the OB (Greer and Shepherd, 1982), then decrease in the final number of newly generated cells incorporated to the *pcd/pcd* OB must also be involved in this effect. Our volumetric analyses indicate significant decreases in the volume of all OB layers studied in the *pcd/pcd* mice (OB total volume reduction, 43.2% ± 5.6%; GL reduction, 25.2% ± 8.0%; EPL reduction, 61.2% ± 5.2%; IML reduction, 40.0% ± 6.8%; $p < 0.01$, mean ± SDM; $n = 11$), with no differences between either age studied (P104 and P150). These data show that the loss of MC elicits a reduction in the total volume of the OB, affecting all layers, including the GCL. The volumetric decrease in the IML must be mainly related to a decrease in the GCL, since this is the largest layer included in the IML. Although the reduction in the GCL was not evident in the OB slices of the *pcd/pcd* mice, our results did point to a decrease in the volume of this layer in the *pcd/pcd* mice, consistent with the decrease in the number of CR+ cells and in the final incorporation of newly generated granule cells in the mutant mice.

DISCUSSION

The present work highlights the role of MC in both radial migration and the survival of newly generated neurons that reach the adult OB. Furthermore, our studies demonstrate that MC are not directly involved in the regulation of the proliferation of neu-

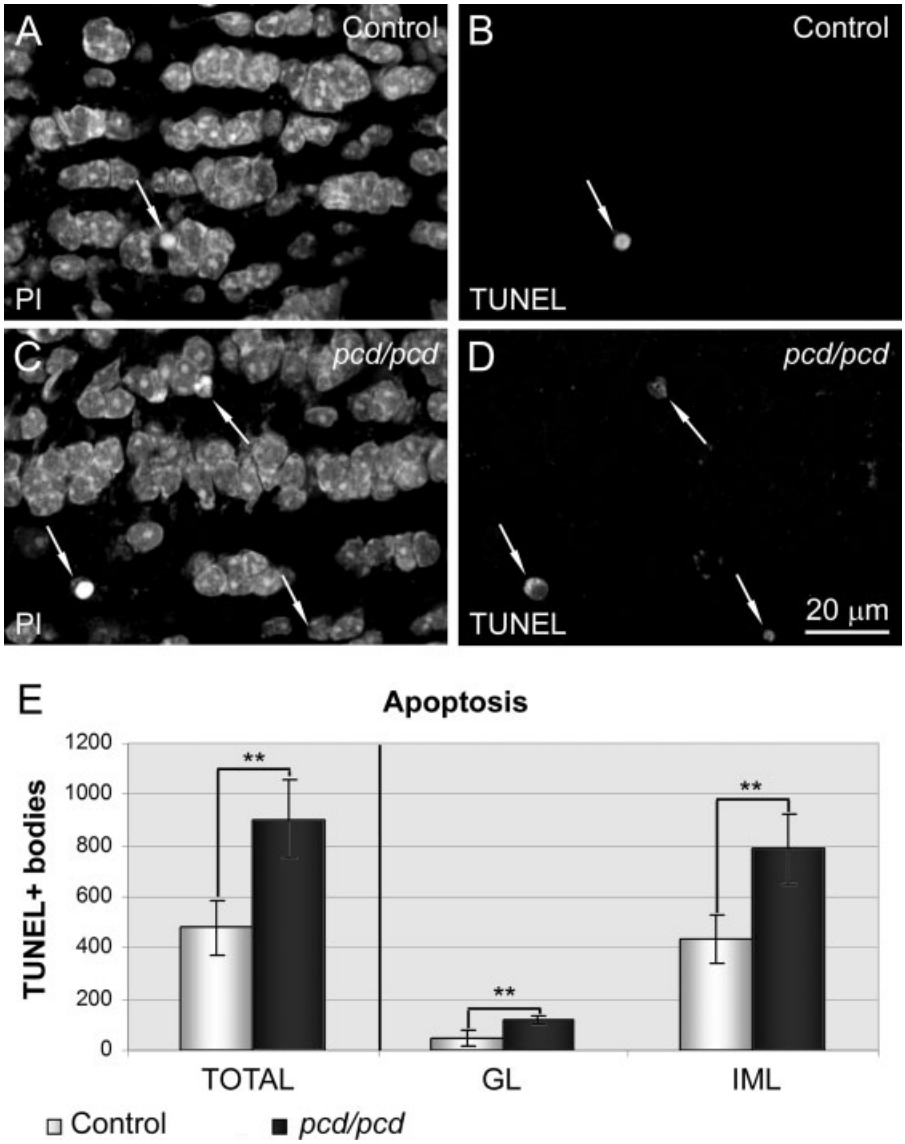

Figure 6 MC loss increases apoptosis in the glomerular and inframitral layers. (A–D) Confocal microscopy images from the IML of a P150 control (A,B) and a *pcd*/*pcd* mouse (C,D) counterstained with PI (A,C) and where TUNEL+ bodies were detected (B,D). The arrows point to TUNEL+ bodies. Note the higher number of TUNEL+ bodies in the IML of the *pcd*/*pcd* mouse (D). Scale bar in (D) applies to (A–C). (E) Quantitative analysis of TUNEL+ bodies in the GL and IML of the control and *pcd*/*pcd* mice. *pcd*/*pcd* mice exhibited a higher number of TUNEL+ bodies in both the GL and IML, indicating that apoptosis increased in these layers. $n = 4$ for control and *pcd*/*pcd* mice. $^{**}p < 0.01$. GL, glomerular layer; IML, inframitral layers.

roblasts of the RMS nor in their tangential migration towards the OB.

Effects of the *pcd* Mutation in the OB

The mechanisms involved in the neuronal degeneration of *pcd*/*pcd* mice are not well known. However, it has been clearly demonstrated that *pcd*/*pcd* mutant mice completely lack *nna1* expression and that other genes are unaffected by the mutation (Fernández-González et al., 2002). Moreover, in the OB, *nna1* mRNA is exclusively expressed by MC (Fernández-González et al., 2002). Thus, possible direct effects of this mutation on other cell populations in the OB are not expected. Although effects of this mutation in

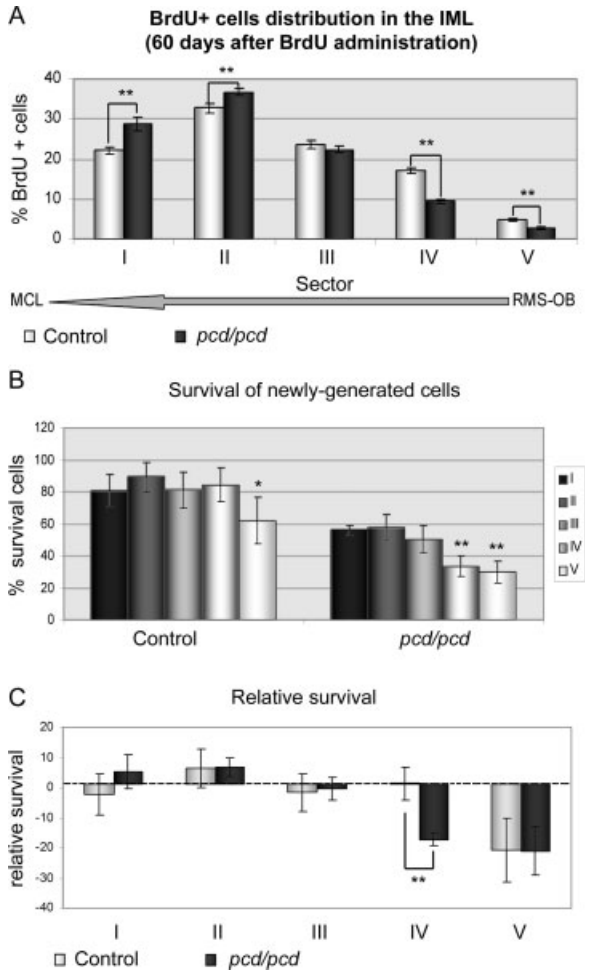

Figure 7 MC loss induces a decrease in the survival of newly-generated cells, changing their final distribution in the inframitral layers. (A) Quantitative analysis of BrdU+ cells distribution in the IML 60 days after BrdU administration. Percentage of BrdU+ cells in each sector is referred to the total number of BrdU+ cells in the IML. In *pcd*/*pcd* mice more newly-generated cells are present in superficial regions (sectors I and II) than in inner ones. Note that the proportion of BrdU+ cells was similar in sector III in the control and mutant mice. (B) Quantitative analysis of the percentage of surviving cells in the IML of control and *pcd*/*pcd* mice. Note that in control animals only sector V exhibited significant differences in cell survival in comparison with the other sectors, whereas in *pcd*/*pcd* mice both sectors IV and V showed significant differences. (C) Quantitative analysis of relative survival. Only sector IV showed significant differences in the relative survival of cells between control and *pcd*/*pcd* mice. Discontinuous line depicts the baseline of relative survival. The baseline of relative survival indicates that the % of surviving cells in this sector is equal to the general % of surviving cells in the whole IML. $n = 4$ for control and *pcd*/*pcd* mice in all analyses. $*p < 0.05$, $**p < 0.01$. MCL, mitral cell layer; RMS-OB, terminal region of the RMS in the caudal OB.

the olfactory epithelium have not been studied directly, some evidence indicates that the sensory input to the *pcd*/*pcd* OB is normal (Greer and Shepherd, 1982; Baker and Greer, 1990). First, the uptake of 2-deoxyglucose to the glomeruli of *pcd*/*pcd* mice shows that the distribution of afferent inputs from olfactory receptor cells is not or only sparingly affected after MC loss (Greer and Shepherd, 1982). Second, TH activity and immunoreactivity are strictly dependent on the olfactory nerve input (Baker et al., 1983, 1993; Cho et al., 1996; Weruaga et al., 2000; Briñón et al., 2001) but remain intact in *pcd*/*pcd* mice (Baker and Greer, 1990). In contrast to the MC, the tufted cells of *pcd*/*pcd* mice are normal (Greer and Shepherd, 1982). Following MC dendrite loss, many of the denervated granule cell gemmules reorganize and establish new synaptic contacts with the remaining mitral and tufted cells (Greer and Halász, 1987). Taking into account this observation, the slower process of deafferentation that occurs during MC loss may be assumed to allow the reorganization of connectivity with unaffected tufted cells in the GL (Baker and Greer, 1990). However, the size of individual glomeruli is reduced in *pcd*/*pcd* mice, and also the relative number of glomeruli per unit area is higher in *pcd*/*pcd* mice (Greer and Shepherd, 1982). EPL width is drastically reduced and its cell density is increased in *pcd*/*pcd* mice (Greer and Shepherd, 1982). These prominent reductions in glomeruli and EPL sizes are most likely due to the loss of MC dendrites (Greer and Shepherd, 1982). Nevertheless, no appreciable alterations in the volume of the GCL or in its cell density have been described previously (Greer and Shepherd, 1982), whereas our results revealed a clear reduction in the number of CR+ cells and the size of this layer. Our survival analysis clearly revealed a reduced final incorporation of newly generated interneurons into the IML. This therefore indicates that in addition to the volumetric alteration caused directly by MC loss, other indirect effects caused by the influx of MC on interneuron regionalization and survival do exist.

MC Loss Does Not Affect Cell Proliferation or Tangential Migration Through the RMS

The presence of *nna1* mRNA, which is completely absent in *pcd*/*pcd* mutant mice, has not been described in adult proliferating cells in control mice (Fernández-González et al., 2002). Therefore, no direct effects of this mutation on these cells should be expected. Our analyses demonstrate that MC loss

Table 6 *pcd/pcd* Mice Exhibit Changes in the BrdU/NeuN Ratio in the GL 60 Days After BrdU Administration but not in the IML Layer

	Layer			
	GL		IML	
Markers	Control	*pcd/pcd*	Control	*pcd/pcd*
BrdU/NeuN	33.5 ± 9.2	56.6 ± 7.7**	95.3 ± 1.0	92.6 ± 3.4
BrdU/CR	41.9 ± 7.7	43.8 ± 8.3	26.4 ± 4.3	28.3 ± 1.3
BrdU/NeuN or CR	68.5 ± 3.1	78.2 ± 5.7*	96.9 ± 0.3	94.1 ± 2.2

Percentage of cells colocalizing BrdU with neuronal markers referred to the total number of BrdU+ cells in each layer. Data represent the mean ± SDM.

*$p < 0.05$ and **$p < 0.01$ versus control data at the same time after BrdU administration. $n = 4$ in all groups.

does not affect proliferation nor tangential migration of cells in the RMS. These result agree with previous studies, indicating that the absence of OB or changes in the arrival of sensory signal to the OB do not affect cell proliferation or tangential migration in the RMS (Frazier-Cierpial and Brunjes, 1989; Kirschenbaum et al., 1999; Petreanu and Álvarez-Buylla, 2002; Rochefort et al., 2002; Yamaguchi and Mori, 2005). All these data suggest that cell proliferation and tangential migration through the RMS are not highly influenced by changes in the OB. Nevertheless, it must be considered that other studies indicate that the interruption of the arrival of the olfactory signal to the OB affects cell proliferation in the RMS, enhancing (Mandairon et al., 2003) or reducing it (Corotto et al., 1994).

MC are Involved in the Radial Migration of Neuroblast Through the OB

Since most neuroprogenitor cells have completed their radial migration 14 days after they are born (Kato et al., 2000; Petreanu and Álvarez-Buylla, 2002) and local cell proliferation within the OB of adult mice is negligible except for the RMS-OB (Lemasson et al., 2005), the number of BrdU+ cells in the OB 14 after BrdU administration must reflect the pool of cells that have migrated tangentially through the RMS to reach the OB. Moreover, only a reduced number of BrdU+ cells was detected in the SVZ or RMS (data not shown), indicating that most of the SVZ or RMS proliferating cells stained with BrdU had finished their tangential migration and had reached the OB. Furthermore, once neuroblasts reach the OB, they migrate radially towards the GCL and GL and acquire mature features, then differentiating into interneurons (Altman, 1969; Lois and Álvarez-Buylla, 1994; Carleton et al., 2003). Thereafter, many of these cells die, mainly during a window time ranging from the 15th to the 30th day after their birth (Kato et al., 2000; Petreanu and Ávarez-Buylla, 2002; Yamaguchi and Mori, 2005).

Studies on the regulation of neuroblast migration through the adult OB are scarce. Interactions between MC and interneurons have been considered necessary for the correct migration of granule cells during development (Whitley et al., 2005). Our results in adult animals are consistent with this previous assumption in the developing OB. Radial migration has been described as not being significantly affected by olfactory deprivation, indicating that it is not regulated by sensory inputs to the OB (Yamaguchi and Mori, 2005). However, other authors have shown that sensory deprivation, and therefore sensory input, affects the expression of some molecules regulating migration: reelin and tenascin-R (Saghatelyan et al., 2004; Okuyama-Yamamoto et al., 2005). Our findings clearly indicate that MC, which directly receive the sensory input in the OB (Mori et al., 1999; Kratskin and Belluzzi, 2003), may influence radial migration. Tenascin-R expression is restricted to the GCL and IPL (Saghatelyan et al., 2004) whereas reelin is expressed by MC, among other cell types (Alcántara et al., 1998; Hack et al., 2002; Pappas et al., 2003). Thus, we considered reelin a better molecular candidate than tenascin-R to explain the migration changes observed in *pcd/pcd* mice. Furthermore, reelin has been suggested to be involved in the interactions between MC and neuroblasts (Whitley et al., 2005). The reelin staining patterns obtained by us are in agreement with previous descriptions in the OB (Hack et al., 2002; Pappas et al., 2003). Defects in migration from the core of the RMS-OB to the GCL occur in *reeler* mice (Hack et al., 2002), which totally lack reelin expression (D'Arcangelo et al., 1995; Pappas et al., 2003). A similar effect could be expected to occur in the *pcd/pcd* OB because of the loss of reelin-producing MC, although this has not yet been observed. This indicates that the synthesis of reelin

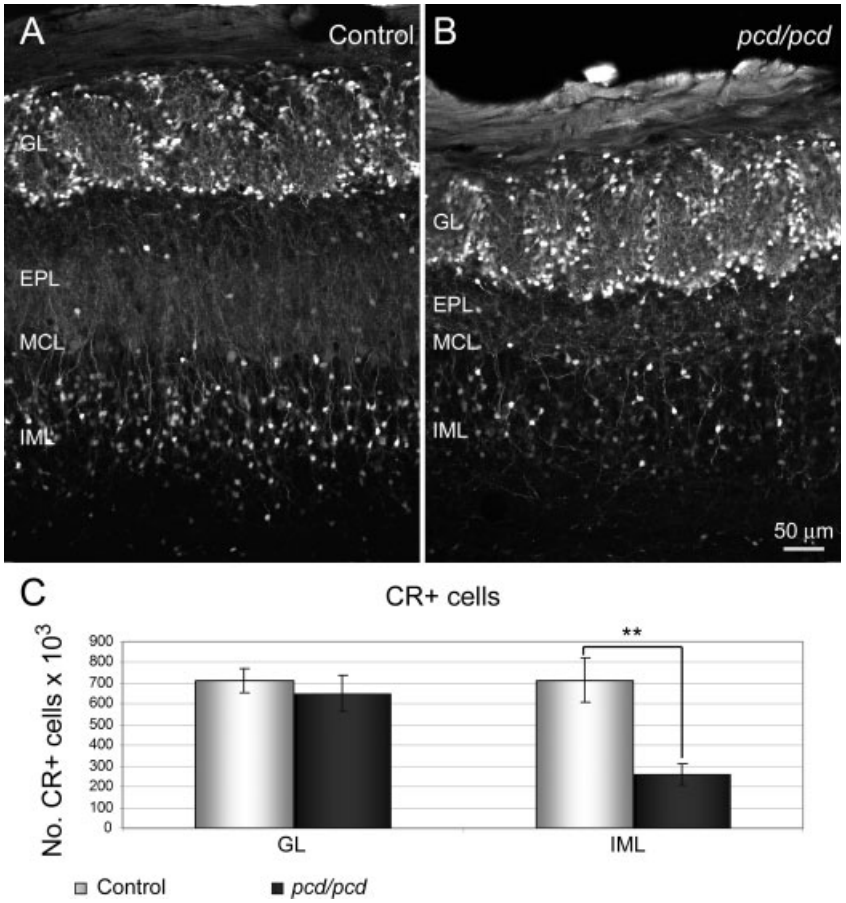

Figure 8 MC loss induces a decrease in the number of calretinin-positive cells in the inframitral layers but not in the glomerular layer. (A,B) Confocal microscopy images from coronal sections from the OB of a P150 control (A) and a P150 *pcd*/*pcd* mouse (B) labeled for CR. CR is expressed in all layers of the OB. Weakly stained MC can be appreciated in the MCL in the control but not in the *pcd*/*pcd* OB. Note the higher density of CR+ cells in the GL and the lower density in the IML for *pcd*/*pcd* mice as compared with controls. Scale bar in (B) applies to (A). (C) Quantitative analysis of CR+ cells in the GL and IML of the control and *pcd*/*pcd* mice. *pcd*/*pcd* mice exhibited a similar number of CR+ cells in the GL and higher in the IML. $n = 4$ for control and *pcd*/*pcd* mice. $^{**}p < 0.01$. CR, calretinin; EPL, external plexiform layer; GL, glomerular layer; IML, inframitral layers; MCL, mitral cell layer.

by MC is not an indispensable requisite for neuroblasts to migrate through the OB. The possible reduction in reelin production brought about by MC loss must be compensated, allowing neuroblasts to migrate normally, or even overcompensated, causing the migrational alterations observed in our study. The actual changes in the gradient of reelin through the *pcd*/*pcd* OB could be involved in such compensatory mechanisms. Two observations suggest a change in the gradient of reelin concentration from the GL to GCL. First, the notable increase in the density of reelin+ cells located in and close to the GL. Second, the reduction in the width of the *pcd*/*pcd* EPL lead the GL and RMS-OB to become closer (Greer and Sheperd, 1982). Furthermore, it has been demonstrated that the GL exerts an attractant effect on the RMS (Liu and Rao, 2003). These data indicate that changes in both cell density and layer widths in the *pcd*/*pcd* OB induced by MC loss could influence the increase in neuroblast migration from the RMS-OB to the GL.

Final Number of Newly Generated Cells in the IML, But Not in the GL, is Reduced by MC Loss

Our analyses demonstrate that about 80% of newly-generated cells survive after their incorporation to the OB. This datum is similar to that obtained in previous

analysis by other authors (Yamaguchi and Mori, 2005). Nevertheless, in another work the estimated survival of newly-generated cells was 50% (Petreanu and Álvarez-Buylla, 2002). Discrepancies between these studies could be due to the different markers of proliferation employed, the different injection protocol used and the different strains of mice used.

The increase in cell death in *pcd*/*pcd* mice (Fig. 9) is in accordance with previous studies, demonstrating that granule cell survival depends on their synaptic connections with mitral and tufted cells (Petreanu and Álvarez-Buylla, 2002; Yamaguchi and Mori, 2005). Nevertheless, studies on factors controlling the survival of periglomerular neurons newly incorporated to the GL in adults are scarce. Our findings clearly indicate that the number of these elements in the GL does not depend on their synaptic contacts with MC. The survival of newborn neurons does depend on the level of synaptic activity that they receive (Corotto et al., 1994; Petreanu and Álvarez-Buylla, 2002; Rochefort et al., 2002; Mandairon et al., 2003; Yamaguchi and Mori, 2005). Thus, the absence of any effect of MC loss on the final number of new cells incorporated into the *pcd*/*pcd* GL [Fig. 9(A)] and on the total number of CR+ cells in the GL [Fig. 8(C)] could be explained in terms of the maintenance of normal levels of activity in the *pcd*/*pcd* glomeruli (see data before about 2-desoxyglucose and TH expression). Newly generated periglomerular cells must establish synaptic contacts with olfactory nerve axons, with tufted cells and with the few remaining MC, which would compensate for the absence of most apical dendrites from MC (Baker and Greer, 1990).

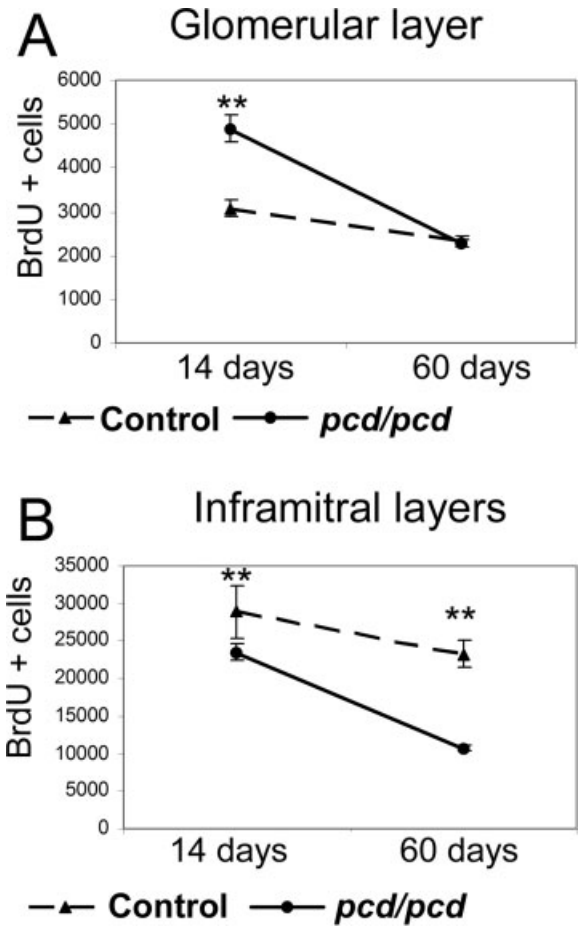

Figure 9 MC loss diminishes the final number of newly-generated cells incorporated into the inframitral layer but not into the glomerular layer. Quantitative analysis of the number of BrdU+ cells in the glomerular layer (A) and inframitral layers (B) of control and *pcd*/*pcd* mice 14 and 60 days after BrdU administration. Note that the number of BrdU+ cells 14 days after BrdU administration was significantly higher in the *pcd*/*pcd* GL compared with the same layer in controls. Moreover, the number of BrdU+ cells in the *pcd*/*pcd* GL diminished and matched the number of BrdU+ cells in the GL of control mice 60 days after BrdU administration. $n = 4$ for control and *pcd*/*pcd* mice. $^{**}p < 0.01$, comparisons were done between control and mutant mice data.

MC Loss Induces a Higher Decrease in the Survival of Newly Generated Cells of the Deeper Regions of the IML

The final internal–external distribution of neurons through the GCL has been proposed to arise from a differential incorporation of new cells rather than from their selective elimination (Lemasson et al., 2005). Our data obtained in control mice clearly demonstrate this assumption. The distribution of BrdU+ cells is maintained from day 14 after BrdU administration (when most arriving cells have concluded their radial migration; Petreanu and Álvarez-Buylla, 2002) to day 60 after BrdU administration [Fig. 10(A–E)]. In this control scenario, the selective elimination of cells did not alter the distribution of newly generated cells, except for the deepest sublayer of IML (sector V). This sector includes the RMS-OB in which some delayed neuroblasts stained with BrdU could still be migrating 14 days after BrdU administration but not 2 months later, which could explain the changes observed in the number of BrdU+ cells in this sector between the ages [Fig. 10(E)]. Nevertheless, selective elimination of newly generated cells plays an important role for the final distribution of cells in *pcd*/*pcd* IML, since it increases internal–external distribution differences [Fig. 10(A–E)]. This indicates that without MC both the final amount and the final distribu-

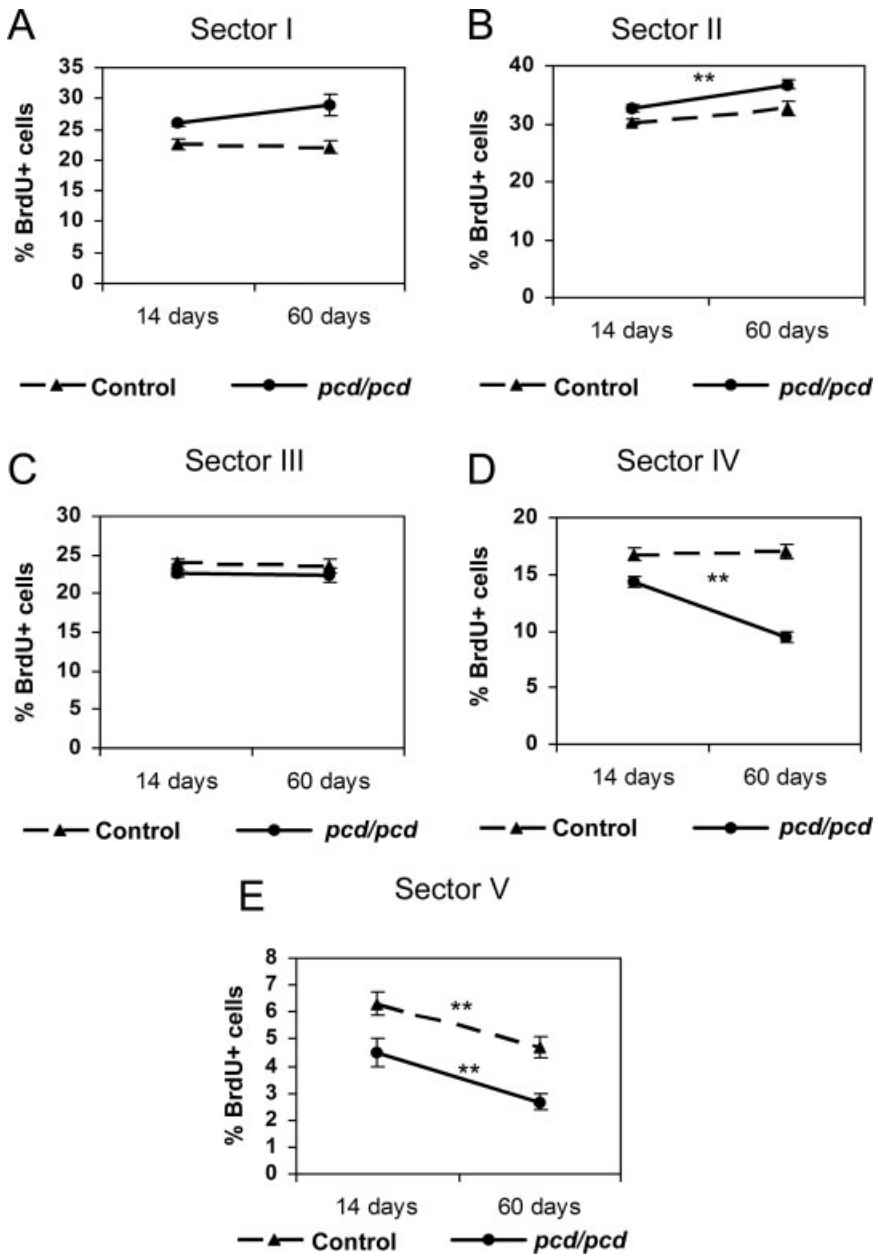

Figure 10 MC loss affects the final distribution of newly-generated cells in the inframitral layers. Quantitative analysis of the distribution of BrdU+ cells in the IML. The percentage of BrdU+ cells within each sector and time is referred to the total number of BrdU+ cells in the IML. Note that in control mice only sector V shows differences in the % of BrdU+ cells between 14 and 60 after BrdU administration. In *pcd*/*pcd* mice, the proportion of BrdU+ cells changed in sectors II (where it increased), IV and V (where they decreased) from 14 to 60 days after BrdU administration. This indicates that MC loss induces changes in the survival of cells, affecting the final distribution of newly-generated cells in the IML, mainly in sectors II and IV. $n = 8$ for control and $n = 7$ for *pcd*/*pcd* mice 14 days after BrdU administration and $n = 4$ for control and *pcd*/*pcd* mice 60 days after BrdU administration. $^{**}p < 0.01$; comparisons were made between the data obtained 14 and 60 days after BrdU administration in control and *pcd*/*pcd* mice, respectively.

tion of precursor cells incorporated at different depths of the IML can be fitted via changes in the survival of newly generated cells. This is consistent with previous studies demonstrating that a reduction in activity and in the number of MC induces apoptosis predominantly in the deeper zone of the GCL (Mandairon

et al., 2003; Koyano et al., 2005). This is also related to the predominance of granule cells connecting with MC (named type II) deeper in the GCL (Greer, 1987; Kratskin and Belluzzi, 2003). Three types of granule cells have been distinguished in the mouse OB according to their different distribution along the GCL and their synaptic connections with mitral or tufted cells (Greer, 1987). The loss of MC induces a general decrease in the survival of newly generated cells throughout the IML that is stronger in the deeper sector of the GCL close to the OB-RMS (sector IV). In contrast, those in the superficial parts are selectively spared, presumably due to their integration in circuits with tufted cells.

To conclude, our findings demonstrate the plastic capacities of the OB, providing new data about the mechanisms involved in adult neurogenesis and the importance of synaptic targets for supporting the arrival and incorporation of newly generated neurons. Understanding the mechanisms involved in adult neurogenesis and functional replacement is mandatory for the development of effective cell replacement therapies against CNS diseases (Shihabuddin et al., 1999; Lie et al., 2004).

We thank Dr. Jozsef Z. Kiss and Eduardo Gascon (Department of Neuroscience, University of Geneva Medical School, Geneva, Switzerland) for their help with the TUNEL technique. We express our gratitude to Dr. J.-L. Guénet, formerly in the Mammalian Genetics Unit from the Institut Pasteur (Paris), for his helpful advice on the genotyping of the animals.

REFERENCES

Alcántara S, Ruiz M, D'Arcangelo G, Ezan F, de Lecea L, Curran T, Sotelo C, et al. 1998. Regional and cellular patterns of reelin mRNA expression in the forebrain of the developing and adult mouse. J Neurosci 18:7779–7799.

Altman J. 1969. Autoradiographic and histological studies of postnatal neurogenesis. IV. Cell proliferation and migration in the anterior forebrain, with special reference to persisting neurogenesis in the olfactory bulb. J Comp Neurol 137:433–457.

Altman J, Das GD. 1965. Autoradiographic and histological evidence of postnatal hippocampal neurogenesis in rats. J Comp Neurol 124:319–335.

Arvidsson A, Collin T, Kirik D, Kokaia Z, Lindvall O. 2002. Neuronal replacement from endogenous precursors in the adult brain after stroke. Nat Med 8:963–970.

Baker H, Greer CA. 1990. Region-specific consequences of pcd gene expression in the olfactory system. J Comp Neurol 293:125–133.

Baker H, Kawano T, Margolis FL, Joh TH. 1983. Transneuronal regulation of tyrosine hydroxylase expression in olfactory bulb of mouse and rat. J Neurosci 3:69–78.

Baker H, Morel K, Stone DM, Maruniak JA. 1993. Adult naris closure profoundly reduces tyrosine hydroxylase expression in mouse olfactory bulb. Brain Res 614:109–116.

Bignami A, Dahl D. 1974. Astrocyte-specific protein and radial glia in the cerebral cortex of newborn rat. Nature 252:55–56.

Briñón JG, Crespo C, Weruaga E, Martínez-Guijarro FJ, Aijón J, Alonso JR. 2001. Bilateral olfactory deprivation reveals a selective noradrenergic regulatory input to the olfactory bulb. Neuroscience 102:1–10.

Carleton A, Petreanu LT, Lansford R, Álvarez-Buylla A, Lledo PM. 2003. Becoming a new neuron in the adult olfactory bulb. Nat Neurosci 6:507–518.

Carleton A, Rochefort C, Morante-Oria J, Desmaisons D, Vincent JD, Gheusi G, Lledo PM. 2002. Making scents of olfactory neurogenesis. J Physiol Paris 96:115–122.

Cho JY, Min N, Franzen L, Baker H. 1996. Rapid downregulation of tyrosine hydroxylase expression in the olfactory bulb of naris-occluded adult rats. J Comp Neurol 369:264–276.

Corotto FS, Henegar JR, Maruniak JA. 1994. Odor deprivation leads to reduced neurogenesis and reduced neuronal survival in the olfactory bulb of the adult mouse. Neuroscience 61:739–744.

D'Arcangelo G, Miao GG, Chen SC, Soares HD, Morgan JI, Curran T. 1995. A protein related to extracellular matrix proteins deleted in the mouse mutant reeler. Nature 374:719–723.

Doetsch F, García-Verdugo JM, Álvarez-Buylla A. 1997. Cellular composition and three-dimensional organization of the subventricular germinal zone in the adult mammalian brain. J Neurosci 17:5046–5061.

Fernández-González A, La S, Treadaway J, Higdon JC, Harris BS, Sidman RL, Morgan JI, et al. 2002. Purkinje cell degeneration (pcd) phenotypes caused by mutations in the axotomy-induced gene, *Nna1*. Science 295:1904–1906.

Frazier-Cierpial L, Brunjes PC. 1989. Early postnatal cellular proliferation and survival in the olfactory bulb and rostral migratory stream of normal and unilaterally odor-deprived rats. J Comp Neurol 289:481–492.

Gascon E, Vutskits L, Zhang H, Barral-Moran MJ, Kiss PJ, Mas C, Kiss JZ. 2005. Sequential activation of p75 and TrkB is involved in dendritic development of subventricular zone-derived neuronal progenitors in vitro. Eur J Neurosci 21:69–80.

Gheusi G, Cremer H, McLean H, Chazal G, Vincent JD, Lledo PM. 2000. Importance of newly generated neurons in the adult olfactory bulb for odor discrimination. Proc Natl Acad Sci USA 97:1823–1828.

Greer CA. 1987. Golgi analyses of dendritic organization among denervated olfactory bulb granule cells. J Comp Neurol 257:442–452.

Greer CA, Halász N. 1987. Plasticity of dendrodendritic microcircuits following mitral cell loss in the olfactory

bulb of the murine mutant Purkinje cell degeneration. J Comp Neurol 256:284–298.

Greer CA, Shepherd GM. 1982. Mitral cell degeneration and sensory function in the neurological mutant mouse Purkinje-cell degeneration (pcd). Brain Res 235:156–161.

Hack I, Bancila M, Loulier K, Carroll P, Cremer H. 2002. Reelin is a detachment signal in tangential chain-migration during postnatal neurogenesis. Nat Neurosci 5:939–945.

Hastings NB, Gould E. 1999. Rapid extension of axons into the CA3 region by adult-generated granule cells. J Comp Neurol 413:146–154.

Hof PR, Young WG, Bloom FE, Belichenko PV, Celio MR. 2000. Comparative cytoarchitectonic atlas of the C57BL/6 and 129/Sv.

Kato T, Yokouchi K, Kawagishi K, Fukushima N, Miwa T, Moriizumi T. 2000. Fate of newly formed periglomerular cells in the olfactory bulb. Acta Otolaryngol 120:876–879.

Kay JN, Blum M. 2000. Differential response of ventral midbrain and striatal progenitor cells to lesions of the nigrostriatal dopaminergic projection. Dev Neurosci 22: 56–67.

Kirschenbaum B, Doetsch F, Lois C, Álvarez-Buylla A. 1999. Adult subventricular zone neuronal precursors continue to proliferate and migrate in the absence of the olfactory bulb. J Neurosci 19:2171–2180.

Koyano KW, Tokuyama W, Miyashita Y. 2005. Deeply located granule cells and mitral cells undergo apoptosis after transection of the central connections of the main olfactory bulb in the adult rat. Neuroscience 131:293–302.

Kratskin IL, Belluzzi O. 2003. Anatomy and neurochemistry of the olfactory bulb. In: Doty RL, editors. Handbook of Olfaction and Gustation, 2nd ed. New York: Marcel Dekker, pp 139–164.

Lemasson M, Saghatelyan A, Olivo-Marin JC, Lledo PM. 2005. Neonatal and adult neurogenesis provide two distinct populations of newborn neurons to the mouse olfactory bulb. J Neurosci 25:6816–6825.

Lie DC, Song H, Colamarino SA, Ming GL, Gage FH. 2004. Neurogenesis in the adult brain: New strategies for central nervous system diseases. Annu Rev Pharmacol Toxicol 44:399–421.

Liu G, Rao Y. 2003. Neuronal migration from the forebrain to the olfactory bulb requires a new attractant persistent in the olfactory bulb. J Neurosci 23:6651–6659.

Lledo PM, Saghatelyan A, Lemasson M. 2004. Inhibitory interneurons in the olfactory bulb: From development to function. Neuroscientist 10:292–303.

Lois C, Álvarez-Buylla A. 1994. Long-distance neuronal migration in the adult mammalian brain. Science 264: 1145–1148.

Lois C, García-Verdugo JM, Álvarez-Buylla A. 1996. Chain migration of neuronal precursors. Science 271:978–981.

Magavi SS, Leavitt BR, Macklis JD. 2000. Induction of neurogenesis in the neocortex of adult mice. Nature 405: 951–955.

Mandairon N, Jourdan F, Didier A. 2003. Deprivation of sensory inputs to the olfactory bulb up-regulates cell death and proliferation in the subventricular zone of adult mice. Neuroscience 119:507–516.

Mori K, Nagao H, Sasaki YF. 1998. Computation of molecular information in mammalian olfactory systems. Network 9:R79–R102.

Mori K, Nagao H, Yoshihara Y. 1999. The olfactory bulb: Coding and processing of odor molecule information. Science 286:711–715.

Mullen RJ, Buck CR, Smith AM. 1992. NeuN, a neuronal specific nuclear protein in vertebrates. Development 116:201–211.

Ogawa M, Miyata T, Nakajima K, Yagyu K, Seike M, Ikenaka K, Yamamoto H, et al. 1995. The reeler gene-associated antigen on Cajal-Retzius neurons is a crucial molecule for laminar organization of cortical neurons. Neuron 14:899–912.

Okuyama-Yamamoto A, Yamamoto T, Miki A, Terashima T. 2005. Changes in reelin expression in the mouse olfactory bulb after chemical lesion to the olfactory epithelium. Eur J Neurosci 21:2586–2592.

Pappas GD, Kriho V, Liu WS, Tremolizzo L, Lugli G, Larson J. 2003. Immunocytochemical localization of reelin in the olfactory bulb of the heterozygous reeler mouse: An animal model for schizophrenia. Neurol Res 25:819–830.

Parent JM, Vexler ZS, Gong C, Derugin N, Ferriero DM. 2002. Rat forebrain neurogenesis and striatal neuron replacement after focal stroke. Ann Neurol 52:802–813.

Peretto P, Merighi A, Fasolo A, Bonfanti L. 1997. Glial tubes in the rostral migratory stream of the adult rat. Brain Res Bull 42:9–21.

Peterson DA. 2002. Stem cells in brain plasticity and repair. Curr Opin Pharmacol 2:34–42.

Petreanu L, Álvarez-Buylla A. 2002. Maturation and death of adult-born olfactory bulb granule neurons: Role of olfaction. J Neurosci 22:6106–6113.

Qin ZP, Ye SM, Du JZ, Shen GY. 2005. Postnatal developmental expression of calbindin, calretinin and parvalbumin in mouse main olfactory bulb. Acta Biochim Biophys Sin (Shanghai) 37:276–282.

Resibois A, Rogers JH. 1992. Calretinin in rat brain: An immunohistochemical study. Neuroscience 46:101–134.

Rochefort C, Gheusi G, Vincent JD, Lledo PM. 2002. Enriched odor exposure increases the number of newborn neurons in the adult olfactory bulb and improves odor memory. J Neurosci 22:2679–2689.

Saghatelyan A, de Chevigny A, Schachner M, Lledo PM. 2004. Tenascin-R mediates activity-dependent recruitment of neuroblasts in the adult mouse forebrain. Nat Neurosci 7:347–356.

Shihabuddin LS, Palmer TD, Gage FH. 1999. The search for neural progenitor cells: Prospects for the therapy of neurodegenerative disease. Mol Med Today 5:474–480.

Somogyi P, Takagi H. 1982. A note on the use of picric acid-paraformaldehyde-glutaraldehyde fixative for correlated light and electron microscopic immunocytochemistry. Neuroscience 7:1779–1783.

Valero J, Berciano MT, Weruaga E, Lafarga M, Alonso JR. 2006. Pre-neurodegeneration of mitral cells in the pcd mutant mouse is associated with DNA damage, transcriptional repression, and reorganization of nuclear speckles and Cajal bodies. Mol Cell Neurosci 33:283–295.

Valero J, Weruaga E, Murias AR, Recio JS, Alonso JR. 2005. Proliferation markers in the adult rodent brain: Bromodeoxyuridine and proliferating cell nuclear antigen. Brain Res Brain Res Protoc 15:127–134.

Weruaga E, Briñón JG, Barbado V, Aijón J, Alonso JR. 1999. A standardized model for the anatomical division of the rodent olfactory bulb. Eur J Anat 3:27–34.

Weruaga E, Briñón JG, Porteros A, Arévalo R, Aijón J, Alonso JR. 2000. Expression of neuronal nitric oxide synthase/NADPH-diaphorase during olfactory deafferentation and regeneration. Eur J Neurosci 12:1177–1193.

Whitley M, Treloar H, De Arcangelis A, Labouesse EG, Greer CA. 2005. The α6 integrin subunit in the developing mouse olfactory bulb. J Neurocytol 34:81–96.

Yamaguchi M, Mori K. 2005. Critical period for sensory experience-dependent survival of newly generated granule cells in the adult mouse olfactory bulb. Proc Natl Acad Sci USA 102:9697–9702.

Zhang RL, Zhang ZG, Zhang L, Chopp M. 2001. Proliferation and differentiation of progenitor cells in the cortex and the subventricular zone in the adult rat after focal cerebral ischemia. Neuroscience 105:33–41.

Zheng W, Nowakowski RS, Vaccarino FM. 2004. Fibroblast growth factor 2 is required for maintaining the neural stem cell pool in the mouse brain subventricular zone. Dev Neurosci 26:181–196.